Analysis of commercial glasses with different strengthening treatments: emphasis on the tin side, defects, structure connectivity and cracking behavior

Carmen M. Fernández-Posada,[a] Andrew R. Barron[a,b,c,*]

[a] *Energy Safety Research Institute, Swansea University Bay Campus, Swansea, SA1 8EN, Wales, United Kingdom*

[b] *Department of Chemistry, Rice University, Houston, TX 77005, USA.*

[c] *Department of Materials Science and Nanoengineering, Rice University, Houston, TX 77005, USA.*

ABSTRACT

Tin side of commercial glasses with different strengthening treatments (i.e. tempered, heat strengthened, chemically strengthened) and without treatment (annealed soda-lime glass) have been compositional and surface characterized and then, compared with Gorilla Glass®. Surface flaws from the strength treatment were observed in thermally treated samples by AFM. Raman studies show differences in the network connectivity (Q^2/Q^1 ratio) because the different structures caused by the treatments. XPS was used to evaluate the oxidation state of the tin and compare the variations through the different treatments. Complementary, a study about the crack behaviour using a Vickers indenter was performed; different cracking pattern was obtained for float soda-lime glass in comparison with Gorilla Glass®. In addition, the IQ^2:IQ^1 ratio as determined from Raman spectroscopy correlates with crack size from indentations.

KEYWORDS: glass; structure; tin-side; indentation; strength, AFM; XPS

*Corresponding author.

E-mail address: a.r.barron@swansea.ac.uk (A. R. Barron)

1. Introduction

Silicate glasses are the most used industrial glasses as the natural occurrence of its components [1]. It represents around the 70% of the glass industry and it is used for various applications such as windshield [2], containers [3], bioactive glasses [4]. Ideal silicate glass can be described as a random three-dimensional network of $[SiO_4]^{4-}$ tetrahedra. Disorder in this structure is introduced by different Si-O-Si angles and rotations of the $[SiO_4]^{4-}$ tetrahedral around the linking O or around the line connecting the linking oxygen with one of the silicon atoms. The disorder is also defined by the existence of bridging oxygen (BO) and non-bridging oxygen (NBO) or terminal species. The addition of other elements changes the connectivity of the Si-O network. For example, optimal properties of soda-lime-silicate glass can be achieved by compositional compromises between Na_2O, which is added to reduce melting temperatures and the amount of CaO, which helps to prevent phase separation and increment its durability [5].

Nowadays, commercial silicate glasses are still called soda-lime silicates even though; they have around six other kinds of oxides added to improve their properties. The most extended method of manufacturing flat soda-lime silicates sheets at the industry is using a tin bath in which the molten glass “floats” with the aim of obtaining uniform thickness of the final product [6]. As a result of the process, “float glass” ends up with one of the sides having tin incorporated (“tin side”) and another one (“air side”) without it or in a very small amount. The tin side is meant to have higher hardness and elastic modulus because the Sn(II)/Sn(IV) acts as a modifier of the network [7]. However, some studies show a tin side of commercially available glasses with similar or lower hardness properties than air side [8,9]. This inconsistency of results has been sometimes attributed to a higher concentration of flaws produced by the rollers used in the heat treatment during its processing or because the studies have been carried out inducing cracks [10].

Multiple methods have been developed to increase the strength in glass [11]. Thermal treatment of glass is a well-established technology for car windshields [12]. Glass from the float process has already been subjected to an annealing treatment [13], but an additional

thermal treatment (650 °C) can increase the strength of the glass (>2×) although also making it more brittle as a consequence. Tempered glass is obtained by doing an air quenching, which allows obtaining higher surface compression. Whereas for heat strengthening glass the cooling down is slower and as a result, the surface compression achieved is lower.

Unfortunately, heat treatments don't work for thin glass as the required temperature gradient through the thickness cannot be obtained. Alternatively, chemical strength methods or ion exchange strengthening have been developed to be used in all range of thickness, and its application is even possible on shaped glass [14, 15]. Ion exchange is the most common industrial process that places the float glass in a vessel containing a molten salt, (usually KNO_3) during several hours at temperatures below the strain point. The K^+ (1.52 Å) exchange places with the smaller Na^+ (1.16 Å) in the surface of the glass. The final strength improvement depends on the concentration of the ions present in the salt bath and its nature, as well as the bath temperature and immersion time [16].

Alkali aluminosilicate glasses (e.g., Corning Gorilla Glass®) with exceptional strength properties have been strengthened by ion exchange in order to satisfy needs of such a glass in electronics devices like the screens of phones [17]. This glass is made by fusion process instead of float glass, which provides a uniform thickness of the glass sheet [18]. Studies of the influence of ion exchange in alkali aluminosilicate glass and float glass suggesting a lower diffusion value of ion-exchange for the latter [19], presumably attributed to tin acting as a block of ion-exchange [20]. However, similar values of final potassium concentration have been obtained for alkali aluminosilicate glass in both sides [19]. No studies investigating the influence of ion-exchange process into the tin side of commercial float glass has been performed prior to the present work.

The surface chemistry of glasses is important as its influences the interaction with coatings and weathering behaviour [21]. The incipient coating technologies (i.e., superhydrophobic, anti-bacterial, and self-cleaning [22]) should be able to work with commercial glasses no matter what supplier of the glass is used and in both sides. This is

because for architectural building applications the instillation is random with regard to tin side or air side being on the outside, and therefore the surface to be coated.

The present study has been performed to shed light about the properties found in commercial glasses with various strengthening treatments. The study was aimed at providing baseline data for the development of coatings able to work in non-ideal conditions of cleanness, for a variety of commercial glasses and to help researches to transfer their technology to the industry [23]. In real-world applications, the majority of these surface treatments result in particulate contamination and/or modification of the top surface [24]. Moreover, home-based applications of coatings won't have a pristine surface before applying the coating. In addition, the crack behaviour of the tin side of the glasses with different strengthening treatments as well as Gorilla Glass® are reported.

2. Materials and Methods

2.1. Materials

All samples were glass square sheets purchased from commercial sources (Table 1).

Table 1

Glasses analysed in this work, their dimensions and suppliers.

Sample	Type	Dimensions (mm)	Thickness (mm)	Supplier
AA1	Annealed float glass	20 x 20	3.0	Stemmerich, Inc., St. Louis, MO USA
AA2	Annealed float glass	20 x 20	1.1	Stemmerich, Inc., St. Louis, MO USA
HS	Heat strengthening float glass	20 x 20	3.85	Stemmerich, Inc., St. Louis, MO USA
T	Tempered float glass	20 x 20	3.85	Stemmerich, Inc., St. Louis, MO USA
CS	Chemically strengthened float glass	16 x 16	0.7	Cat-i Glass, South Elgin, IL USA
GG	Chemically strengthened alkali aluminosilicate (Corning Gorilla Glass®)	16 x 16	0.55	Cat-i Glass, South Elgin, IL USA

2.2. Characterization methods

The morphology of the samples was studied by a JPK NanoWizard II atomic force microscope (AFM) using tapping mode and RTESP-300 (Bruker tips) at a scan rate of 0.5-1 Hz and an image resolution of 512 × 512 pixels. The images were processed and analysed using Gwyddion software.

The composition of the samples was obtained by X-ray analyser (Inca X-ray analysis system, Oxford Instruments, Abingdon, UK), which is coupled with a Hitachi TM3030 bench-top scanning electron microscopy (SEM). Three different sites were measured to get average values and its standard deviation. X-ray photoelectron spectroscopy (XPS) analysis was carried out using a Kratos AXIS Supra (Kratos Analytical, Manchester, UK) spectrometer operating in the constant analyser energy mode. A monochromatic Al-K_α source (1486.74 eV) and a charge neutraliser were used. Survey scans were acquired using pass energy of 160 eV and high-resolution data at a pass energy of 20 eV. Three spectra at room temperature from different areas of the sample were acquired and then normalised. The energetic position of the C 1s emission line (binding energy of 284.6 eV) was chosen to calibrate the energy scale of the spectra. CASA XPS software was used to analyse each spectrum, using a Gaussian-Lorentzian curve fitting (GL(70)) and Shirley-type background.

The Si-O network was studied by un-polarised Raman spectroscopy measured on a Renishaw inVia Reflex Raman Spectrometer System. The excitation source was a 485 nm line at power levels of 100% and as an average of 100 scans for each sample. The instrument enables collecting shifts in Raman band position within an error of ±0.02 cm^{-1}. LabSpec software was used for the deconvolution of the peaks obtained in each spectrum using a Gaussian-Lorentzian curve fitting and a linear baseline was subtracted from all the spectra collected.

Crack indentation behaviour Vickers indentation hardness using 5 kg, dwell 10 s measures were carried out by the hardness test instrument NEXUS 4303. Images of the cracks obtained where taken using a Zeiss Reichart optical microscope and Hitachi TM3030 bench-top SEM in backscattering mode and charge-up reduction mode using 15 kV was used. The later process of the SEM images was carried out by 3D Viewer software in order to

measure the depth of the cracks. Three measures were performed for each sample to get an average and its standard deviation of the values obtained.

3. Results and discussion

3.1. Surface defects analysis

Fig. 1 shows the AFM images recorded and the average roughness (Ra) of the tin side for all the samples listed in Table 1. AFM is very sensitive to dirtiness and many particles appeared because the sample was not previously cleaned. The roughness of all samples is quite dependent on how the samples are cleaned and free from organic contamination. Since we are interested in the surface performance of glass in the state that it would be found prior to secondary *in-situ* treatment, the only reliable observation is the flaws observed in the samples, because these are not artefacts of surface contamination. However, we note that CS is the roughest sample (Ra = 2.14 ±0.27 nm, see Fig. 1e) and shows additional circular abrasions not seen in the other samples, probably due to the ion exchange process. The flattest surface was observed for GG (Ra = 0.27 ±0.07 nm, Fig. 1f) because it is made by fusion process instead of regular float glass [13,18].

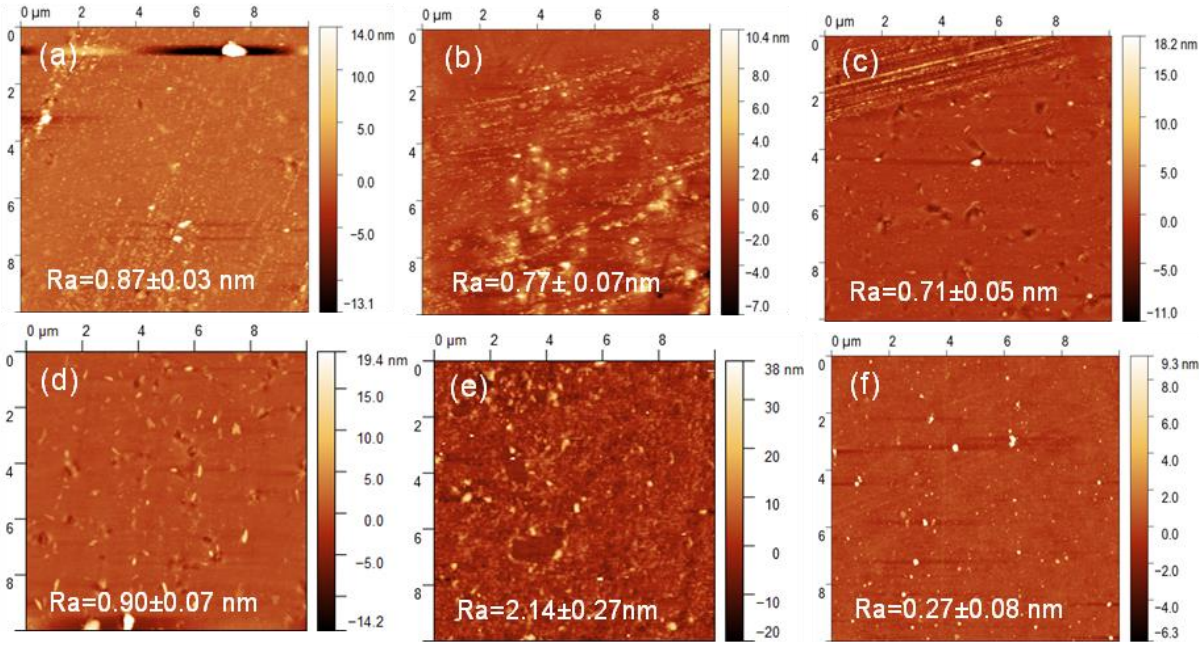

Fig. 1. AFM images, average roughness (Ra) and its standard deviation obtained after the measurement of 3 lines across the image for the tin side of regions (10 x 10 μm) of (a) AA1 (b) AA2 (c) HS (d) T (e) CS and (f) GG.

The average and distribution of flaw size and depth are shown in Fig. 2. The two AA samples show similar flaw size and depth; however, the distribution of flaw depth is decreased with increased thickness of the glass. T glass shows a statistical increase in the size of the flaws, but a decrease in their average depth. The CS sample shows a significant increase in the size and depth of the flaws, especially when compared to the T sample of similar thickness (3.85 mm).

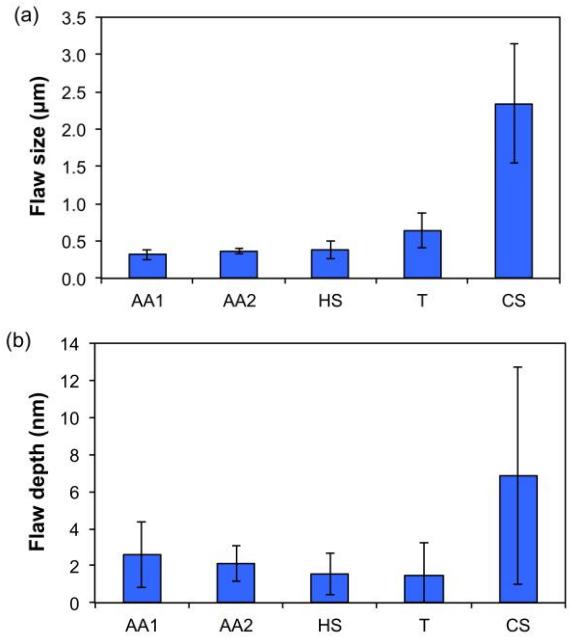

Fig. 2. Average size (a) and depth (b) of flaws as determined from AFM measurements for the tin side of glass samples, with the distribution shown by error bars. Note: the GG samples showed no measurable flaws.

3.2. Compositional analysis

Table 2 shows the average atomic percentage values obtained at 3 different sites of each kind of glass analysed and for tin and air sides obtained using EDX. Considering the same

kind of glass, no significant difference between tin side and air side is observed except for the obvious addition of Sn on the former. For similar glasses (i.e., AA1 versus AA2) there is a correlation between Sn content and the thickness of the samples (Table 2), as would be expected since the thickness of the sample influences the incorporation of tin by the SnO_2 bath.

Table 2

Atomic percentage obtained by EDX for both sides of the as received glass samples.

Sample	Side	O	Si	Na	Ca	Mg	Al	K	S	Sn
AA1	Air	61.69	24.27	8.88	2.86	2.02	0.30			
		±0.18	±0.16	±0.05	±0.06	±0.04	±0.04			
	Tin	61.56	23.64	8.75	3.03	1.99	0.33			0.70
		±0.36	±0.33	±0.03	±0.08	±0.36	±0.16			±0.10
AA2	Air	61.79	23.92	8.32	2.40	2.38	1.05	0.15		
		±0.37	±0.06	±0.19	±0.03	±0.08	±0.54	±0.03		
	Tin	61.71	23.93	8.49	2.57	2.35	0.74			0.22
		±0.30	±0.20	±0.21	±0.01	±0.04	±0.19			±0.02
HS	Air	61.68	24.59	8.47	2.84	1.78	0.52	0.09	0.03	
		±0.12	±0.07	±0.05	±0.01	±0.03	±0.03	±0.01	±0.04	
	Tin	61.22	24.18	8.71	3.07	1.79	0.51			0.53
		±0.03	±0.04	±0.03	±0.03	±0.03	±0.01			±0.03
T	Air	61.50	24.65	8.38	2.95	1.76	0.48	0.11	0.08	
		±0.11	±0.07	±0.02	±0.03	±0.02	±0.02	±0.01	±0.07	
	Tin	61.76	23.68	8.68	2.95	1.76	0.49	0.10		0.58
		±0.23	±0.13	±0.04	±0.02	±0.02	±0.02	±0.09		±0.06
CS	Air	61.82	24.25	3.71	2.44	2.33	0.84	4.63		
		±0.12	±0.05	±0.10	±0.02	±0.02	±0.15	±0.07		
	Tin	62.17	23.75	3.65	2.37	2.27	0.79	4.62		0.39
		±0.16	±0.11	±0.01	±0.04	±0.04	±0.01	±0.05		±0.03
GG	Air[a]	63.54	19.81	2.85		0.72	7.77	5.31		
		±0.11	±0.03	±0.01		±0.02	±0.05	±0.05		

[a] No tin side is present for the GG sample.

A small amount of sulphur was found in the thermally treated samples (T and HS). Although it is not ordinarily related to the thermal treatment, it is more likely a function of the particular manufacturer's process. Sulphur is normally added as a refining agent in the float glass melting furnace, usually in the form of Na_2SO_4 or gypsum ($CaSO_4$) [25], reacting

with the soda in the glass to form a protective layer. It usually washes out at the end of the process but sometimes is retained in the glass composition as a small percentage as SO_3. The CS sample has low sodium content and high potassium content even in the tin side suggesting that the ion-exchange process occurs more or less in a similar level despite the tin. GG is an alkali aluminosilicate glass and, as expected, high levels of aluminium and low levels of sodium and magnesium, and no calcium was found. The process of fabrication of GG incorporates an ion exchange strengthening as evidenced by the high quantities of potassium [19].

Previous research suggests the presence of mix valence tin (i.e., Sn(IV)/Sn(II)) [19,26-28], but the valence ratio in the samples is important because Sn(IV) is reported to increase the connectivity of the glass structure (and hence the hardness) more than Sn(II) [26]. Many factors (composition, thickness, treatment, quality of the surface) influence the glasses in this study, therefore, the Sn(IV)/Sn(II) ratios were calculated from the high-resolution Sn 3d XPS curve fitted spectra for each glass (Fig. 3). It is worthy to mention that the Sn $3d^{3/2}$ peak overlaps with Na KLL Auger peaks [29]. Such peaks have a non-regular shape but they don't contribute to the calculus of the elemental composition. An anomalous survey spectrum was found for annealed thick glass (AA1, Fig 3a), in which all the peaks are doubled. This phenomenon is due to different charging environment of the elements (all these doubled peaks have a Δ ~2 eV respect to the position that it should be) [30]. As a result, it was not possible to obtain reliable calculations of Sn(IV):Sn(II) ratio.

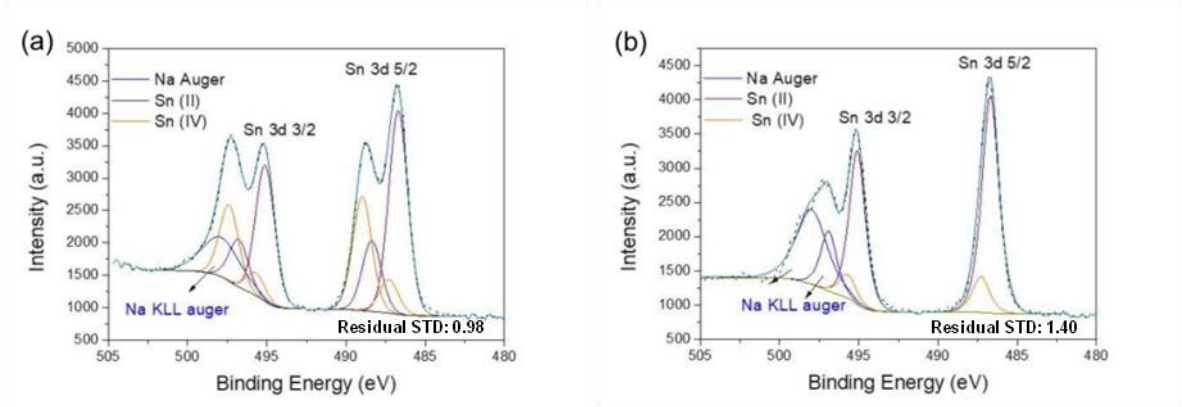

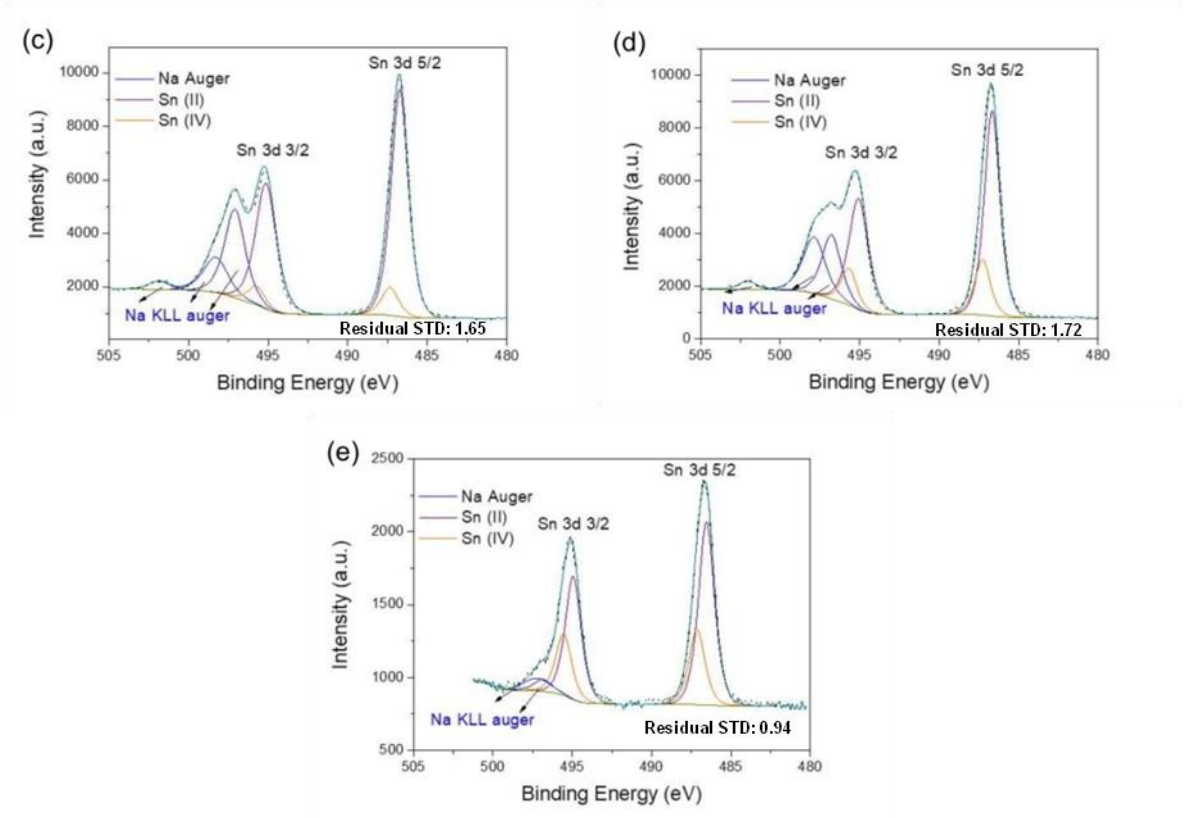

Fig. 3. High resolution Sn 3d spectra peak fit for tin side of (a) AA1, (b) AA2, (c) HS, (d) T, and (e) CS glass samples. The black curves are the experimental data, the lines with different colours correspond to the fitting of the experimental data. The residual standard deviation obtained from the model used is shown for each sample.

The highest Sn(IV):Sn(II) ratio was found for chemical strength glass (Table S2, see Supplementary Material). This is consistent with previous reports that the oxidation of Sn(II) to Sn(IV) results after the ion-exchange treatment [19]. Tempered glass seems to have also higher amount of Sn(IV) that could be related with the high temperature of the thermal treatment [31] followed by the rapid cooling that stabilizes a greater amount of oxidized species. However, heat strengthening seems to have an even lower amount of Sn (IV) than annealed glass. This fact could be related to the stability of the valences states in the glass. If Sn(II) is more stable a slow cooling in the furnace will favour its formation over the other valence states.

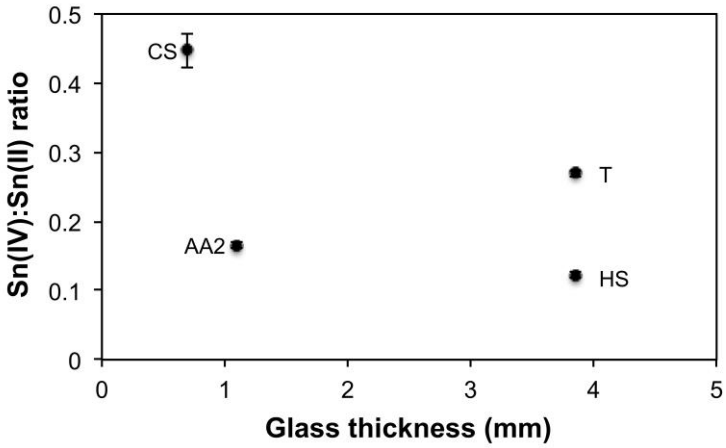

Fig. 4. Plot of Sn(IV):Sn(II) ratio with its error bars as determined by XPS as a function of glass thickness (mm) for AA2, HS, T, and CS glass samples.

The XPS survey analysis of all the glass samples is given in Table S2. The elemental composition of the glass varies between EDX and XPS analysis. EDX values in Table2 are an average of three different spots of around 100 x 100 μm with a depth of 1-2 μm, providing a near bulk composition. In contrast, XPS analysis over a 700 x 300 μm spot size with a few nm in depth, i.e., surface analysis. XPS analysis indicates that the GG sample, while not containing Sn, has an Al:Si ratio of 0.527 ±0.014, and Na:Al ratio of 0.212 ±0.022, showing an aluminium rich surface of this glass.

3.3. Network connectivity

In order to understand the crystallization behaviour of silicate melts, as well as properties such as viscosity, density, and compressibility, it is necessary to know the proportions of the structural units that occur in the glass samples. Such information can be obtained from the analysis of Raman spectrum as the area ratios of individual bands can be related to relative abundance of the associated structural units [32].

Fig. 5 shows all the spectra obtained for the tin side of the samples received which have been recorded between 400 - 1500 cm^{-1}. The thicker samples (AA1, HS, T) present a spectrum with more noise and lower intensity than thin ones (AA2, CS, GG). This observation is related to the higher surface stresses in the thick samples in comparison with

the thin ones. Table 3 present the width of the main peak envelope obtained for the different glasses. The increase of the width of this band is related with the relative order of the Si-O network; it becomes wider when the sample shows high disorder of the network in the form of bond length and/or angle fluctuations [33]. It should also be noted that the spectrum for AA1 shows a higher intensity of the band at 780 cm^{-1}. This band has been suggested to be due to either Si motion in the oxygen tetrahedral environment [34], a stretching motion Q^0 [NBO/Si = 4] [35,36], or a Si-O-Si symmetric stretching of bridging oxygen [BO] between tetrahedra [37].

Table 3

Width of the main peak envelope at 1090 cm^{-1} in the Raman spectra of glass samples.

Sample	Envelope width (cm^{-1})
AA1	162.20
AA2	248.06
HS	228.85
T	233.23
CS	250.62
GG	252.37

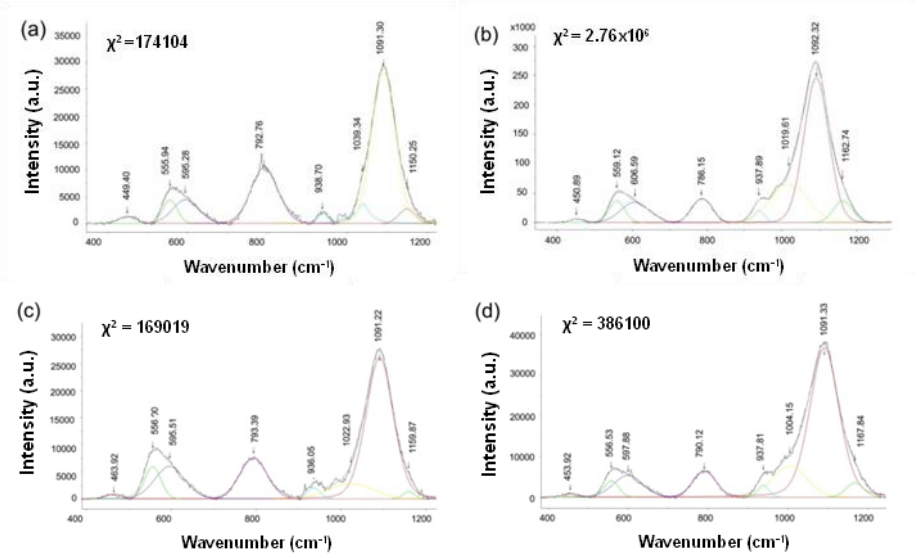

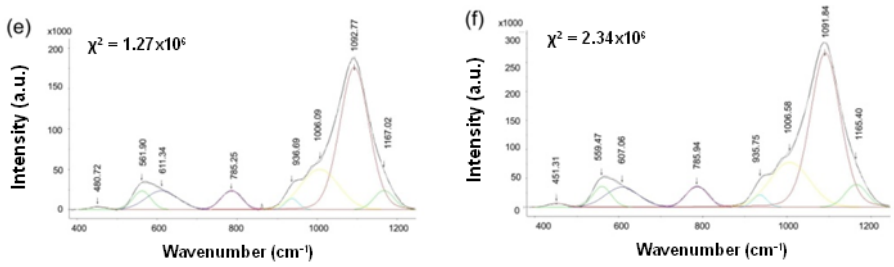

Fig. 5. Raman spectra and curve fit of raw data collected for the tin side of (a) AA1, (b) AA2, (c) HS, (d) T, (e) CS, and (f) GG glass samples. The black curves are the experimental data, the linear red line is the baseline, the curves with different colors correspond to the Gaussian-Lorentzian fit to the experimental data by using Labspac software. X^2 of the fitting displayed for each spectrum.

All glasses show high intensity of the stretching mod envelope (800 – 1200 cm^{-1}), which is characteristic of networks containing a large quantity of alkali and alkaline earth modifiers, which breaks the Si–O-Si links [BO]. This band was fitted using four peaks (950, 1020, 1090 and 1150 cm^{-1}), which are reported to correspond to Si–O stretch vibrations in specific structural units. The band ~950 cm^{-1} is assigned to vibration in Q^1 (NBO/Si = 3); the band ~1020 cm^{-1} is usually correlated with vibration in Q^2 (NBO/Si = 2) and can be also assigned to a vibration in structural units with the metal cations; the most intense band centred ~1090 cm^{-1} come from vibrations in Q^3 (NBO/Si = 1). The final band ~1150 cm^{-1} is related with stretch vibrations of Q^4 (NBO/Si = 0) or Q^3 units with two different neighbours [38-40]. All samples show large half-width which is expected for glasses [32]. Frequencies, area % and intensities of Raman bands obtained from their deconvolution are listed in Table 4.

Table 4

Frequencies (ν, cm^{-1}), relative area (%), and intensities (I) of Raman bands assigned to the structural units present in the glass samples.

Sample		Q^0 (or Si motions in oxygen cage)	Q^1	Q^2	Q^3	Q^4
AA1	ν (cm^{-1})	792.76	938.7	1039.34	1091.3	1150.25
	%A	21.85	1.44	5.38	52.78	10.19

	I	68.04	23.38	39.18	58.14	41.5
AA2	ν (cm^{-1})	786.15	937.9	1019.61	1092.32	1162.74
	%A	6.48	1.91	20.51	52.27	5.79
	I	52.3	30.92	100.2	67.1	49.84
HS	ν (cm^{-1})	793.39	936.05	1022.93	1091.22	1159.87
	%A	14.12	1.79	8.92	54.20	1.94
	I	64.43	29.32	106.28	66.08	26.67
T	ν (cm^{-1})	790.12	937.82	1004.15	1091.33	1167.84
	%A	7.48	1.68	13.90	62.25	3.28
	I	57.12	27.58	86.44	75.29	43.92
CS	ν (cm^{-1})	785.26	936.69	1006.09	1092.77	1167.02
	%A	4.81	1.84	19.76	56.53	5.0
	I	50.17	32.44	94.61	73.8	49.77
GG	ν (cm^{-1})	785.95	935.75	1006.58	1091.84	1165.4
	%A	4.85	1.84	20.20	55.75	5.64
	I	50.66	32.42	95.24	72.68	52.03

Polymerization index (I_p) is defined as the ratio area between the bending and stretching envelopes, Eq. 1), where A_{500} and A_{1000} correspond to the bending bands around 500 cm^{-1} and 1000 cm^{-1}, respectively. This index has been used in a number of reports to classify glassy materials [36,41]. The I_p values (Table 5) indicate that all glasses belong to "Family 1", which corresponds to glasses with a high number of modifiers breaking a large number of Si-O-Si links, i.e., high NBO, low BO. For this class of glass, the Q^2/Q^1 ratio is used instead of I_p, for comparing the extent of polymerization [36]. The higher the number of Q^2 species, the higher the densification of the material, and the higher interconnectivity, by contrast, isolated species means low connectivity. The more free space in the glass network is occupied the higher becomes the density, which leads to an increase in hardness as is proved below [41,42]. As would be expected, there is a linear correlation between Ip and the Q^2/Q^1 and the Q^2/Q^3 ratios confirming the extent of polymerization's dependence on BO (Fig. S1, see Supplementary Materials).

$$I_p = A_{500}/(A_{1000} \times A_{500}) \quad (1)$$

Table 5

Polymerization index (I_p) areas ratio (AQ^2/AQ^3, AQ^2/AQ^1) and intensities ratio (IQ^2/IQ^3, IQ^2/IQ^1) as determined from Raman spectroscopy of the different structural units present in the glass samples.

Sample	I_p	AQ^2/AQ^3	AQ^2/AQ^1	IQ^2/IQ^3	IQ^2/IQ^1
AA1	0.24	0.10	3.75	0.13	1.84
AA2	0.16	0.39	10.72	0.27	3.28
HS	0.30	0.16	4.98	0.10	1.36
T	0.13	0.22	8.26	0.21	2.62
CS	0.14	0.34	10.71	0.28	3.65
GG	0.13	0.36	10.99	0.29	3.71

GG shows the lower number of Q^1 (NBO/Si = 3) being the sample the more polymerized structure. It should be noted that the difference between AA1 and AA2 (Table 5) would suggest that thicker samples have a lower IQ^2/IQ^1 ratio (i.e., less polymerized); however, the extent of polymerization (GG > CS > AA2 > T > AA1 > HS) seems more related to the treatment than the thickness (GG < CS < AA2 < AA1 < HS = T). Furthermore, considering samples with a strengthening treatment, the more Sn(IV) implies more polymerization of surface as can be seen in Fig. 6.

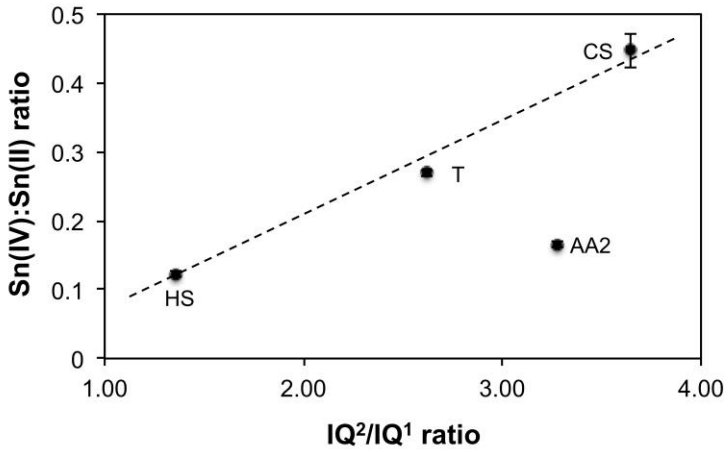

Fig. 6. Plot of IQ^2/IQ^1 ratio as a function of the Sn(IV):Sn(II) ratio with the error bars. A line is drawn as guides to the eyes.

3.4. Crack indentation behaviour

Analysis of the crack dimension obtained by applying 5 kg of load in the tin side of the glasses (and GG) was investigated to establish a mechanical-structural relationship. Fig. 7 represents the indentation imprint obtained because the Vickers indenter as the lateral cracks normally achieved in glass samples

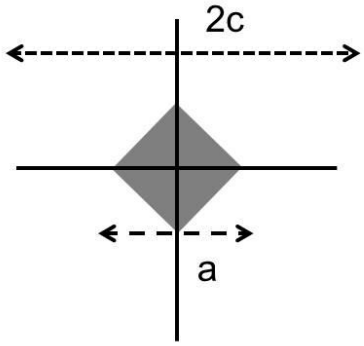

Fig. 7. Schematic representation of the crack generated after applying a Vickers indentation to the glass surface showing the full crack length (2c) and the diagonal of the crack (a).

A representative set of images obtained with an optical microscope of the indentation cracks after applying the load is showed in Fig. 8. Table 6 shows the averages values of the diagonal of the full crack *2c*, the diagonal of the indentation crack *a* (see Fig. 7), and depth of the crack, all of them obtained from SEM for more precision and analysed by 3D-Viewer software (see Fig. 9). The average values of the diagonals consider horizontal and vertical diagonal. Values of the hardness were obtained directly from the instrument.

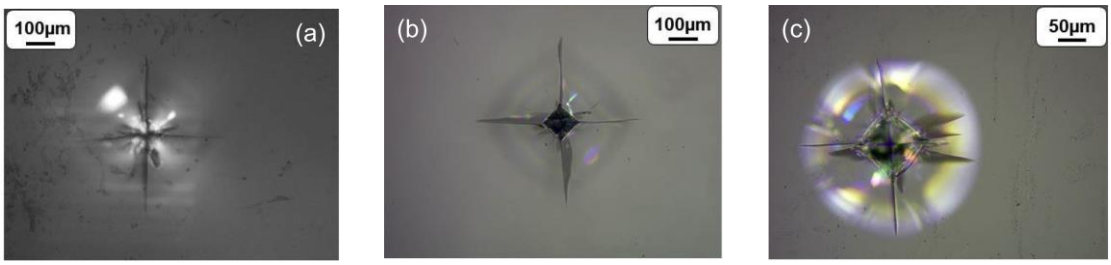

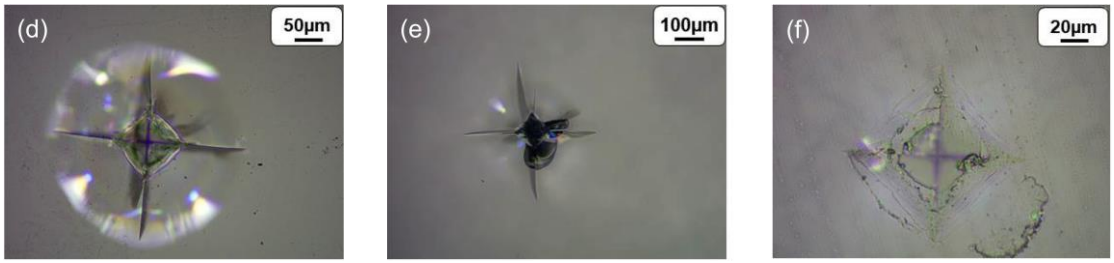

Fig. 8. Cracks obtained by Vickers indentation applying a load of 5 kg in the tin side of (a) AA1, (b) AA2, (c) HS, (d) T, (e) CS, and (f) GG (air side).

Table 6

Crack measures and standard deviations obtained by SEM and hardness for the different glasses analysed

Sample	Lateral crack (2c) (µm)	Vickers indent (a) (µm)	Depth of the crack (µm)	Hardness (GPa)
AA1	558.13 ±29.40	124.83 ±4.45	10.41 ±0.90	4.86 ±0.21
AA2	590.13 ±15.83	133.38 ±3.37	12.53 ±0.90	5.42 ±0.25
HS	312.92 ±21.88	123.35 ±1.41	10.59 ±0.75	5.39 ±0.04
T	316.92 ±10.57	129.87 ±3.52	11.83 ±0.66	5.17 ±0.10
CS	466.85 ±6.97	119.78 ±3.92	13.42 ±0.50	5.37 ±0.14
GG	0	117.76 ±3.56	12.18 ±2.16	6.03 ±0.14

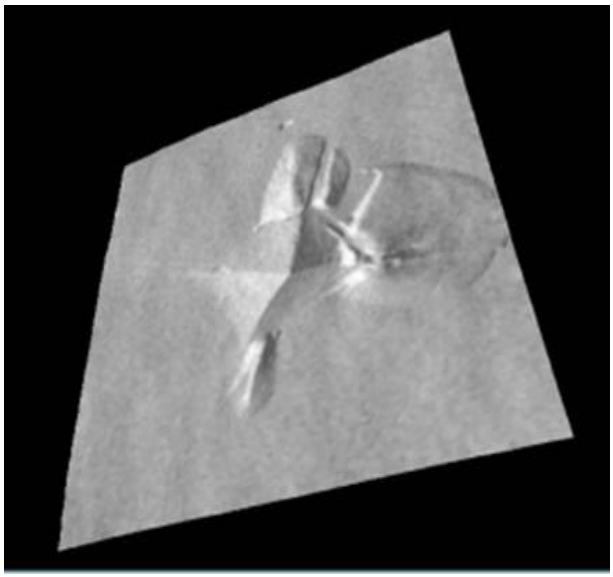

Fig. 9. Representative 3D visualization of Vickers indentation after applying a load of 5 kg to the tin side of CS.

The GG sample doesn't show lateral cracks (Fig. 8f), although a significant range of indentations is made despite having the higher hardness due to the high aluminium content. The heat-treated glasses (T and HS) show a significant diminution of the lateral cracks (2c in Fig. 7) in comparison to the annealed samples (AA1 and AA2) as well as better crack resistivity than CS in a similar manner that has been reported for the air side [42]. There are no correlations observed between the lateral of the crack (2c in Fig. 7) or diagonal of the crack (a in Fig. 6) and depth of the crack or the hardness of the glass. Furthermore, there is no correlation between original flaw size and the induced the cracks measured hardness of the glasses increases with increase IQ^2/IQ^1, although the HS sample is harder than expected.

The one distinct relationship that is observed is the depth of crack increases with increase IQ^2/IQ^1 ratio (i.e., more polymerized). As shown in Fig. 9 there is a good correlation, despite the wide range of data for GG. A similar correlation ($R^2 = 0.79$) is observed for the IQ^2/IQ^3 ratio, suggesting that maximisation of the Q^2 species (NBO/Si = 2) is key in minimising crack depth. As would be expected, therefore, the depth of crack increases with decreasing I_p, but the correlation is not as good ($R^2 = 0.63$). It may be postulated that the depth of crack relates to the deformation of the glass, which would be expected to decrease with increased polymerization of the glass; however, the depth of the crack does not relate to hardness of the glass.

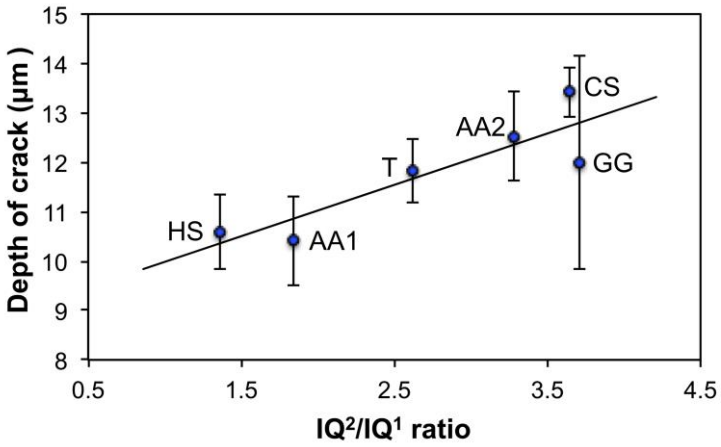

Fig. 9. Plot of the depth of the crack (µm) with error bars obtained by Vickers indentation applying a load of 5 kg as a function of the IQ^2/IQ^1 ratio. The solid line is a linear fit to the experimental data with $R^2 = 0.92$.

Consideration of the non-chemically strengthened glasses (i.e., AA1, AA2, HS, and T) there is a direct correlation between Vickers indent (a) and IQ^2/IQ^1 ratio (Fig. 9). Based upon the IQ^2/IQ^1 ratio of the chemically treated glasses (CS and GG) suggests that without the treatments employed, they would have a crack formation comparable to annealed float glass, i.e., the original source of the glass employed. Regarding the Sn(IV):Sn(II) we find that the sample with the smaller Vickers indenter crack is the one with higher Sn(IV) content, that is the chemical strengthening glass. However, compressive stress of the surface plays definitely a role in the mechanical properties [42] as the thermally treated glass (HS and T) are the ones with smaller lateral cracks. In addition, the surface quality of the sample (number of flaws) definitely may have an impact on the mechanical properties and makes it difficult to establish other patterns.

4. Conclusions

For the first time, the tin side of different commercial float glasses with a variety of strengthening treatments has been compared to standard annealed float glass and Gorilla Glass®. Surface defects in the glass have diverse origins: manufacturer related, shipping and manipulation. Pick out defects can be obtained in the tin side if the glass gets stuck into the

rollers during the thermal treatment. These defects are clearly observed by AFM for heat treated float glass, for tempered samples and for heat strengthening glass but none or few was found for annealed float glass or float glass with chemical strengthening. The debate about the weakness of the tin side of float glass seems to be clearly due to a different kind of surface quality depending on the supplier that could provoke pick out defects also in float glass without any strengthening treatment. The presence of these defects should be tried to avoid by the commercial manufacturers in order to get high strength glass. In addition, everyone working on coating technology should keep in mind that a fraction of the glass used over their product will contain these kinds of defects.

Raman analysis has been proven to be a valuable technique for the calculation of the Si-O species present into the glass as it takes into account directly the different Si-O vibrations. The polymerization of the Gorilla Glass® is the highest one due to the presence of huge amounts of aluminium that contributes to having more connectivity in the glass network by reducing the number of NBO. Chemically strengthening float glass, heat strengthening float glass and tempered float glass show higher polymerization than annealed float glass, as the number of Q^2 species is higher. For the first time, we report a correlation between the Q^2 species and the indent size caused by indentation.

The presence of Sn(IV) in all samples, with the exception of Gorilla Glass®, was determined by XPS analysis. Chemically strengthening float glass and tempered float glass are the ones with higher Sn(IV) amount and it is correlated with the high Q^2 number/polymerization of the glass. Heat strengthening float glass show less Sn(IV) quantity than annealed glass, in agreement with the low polymerization according to Raman analysis.

The higher glass connectivity the more hardness surface is achieved, the strengthening methods provide an improvement into the resistance to lateral cracking after applying a localized forced in the tin side as well. Finally, chemical routes to increase the relative number of Q^2 species should be the focus of research on post-fabrication strengthening treatment.

Acknowledgement

Financial support was provided by Innovate UK (132473), with additional support from Flexible Integrated Energy Systems (FLEXIS) and Reduce Industrial Carbon Emissions (RICE) research operations funded by the Welsh European Funding Office (WEFO), the Sêr Cymru Chair Programme, and the Robert A Welch Foundation (C-0002). We would like to acknowledge the assistance provided by the Swansea University AIM Facility, which was funded in part by the EPSRC (EP/M028267/1), the European Regional Development Fund through the Welsh Government (80708) and the Sêr Solar project via the Welsh Government. Dr Daniel Jones is acknowledged for the XPS data collection. Vince Pugliese, Erik Koep and Jay Rothenberger (C-Bond Systems) are acknowledged for supplying the glass samples and useful discussions. The authors declare no conflict of interests.

References

[1] D.R. Neuville, Viscosity, structure and mixing in (Ca, Na) silicate melts, Chem. Geol., 229 (2006) 28-41. DOI: 10.1016/j.chemgeo.2006.01.008.

[2] J. Schneider, S. Schula, W.P. Weinhold, Characterisation of the scratch resistance of annealed and tempered architectural glass, Thin Solid Films, 520 (2012) 4190-4198. DOI: 10.1016/j.tsf.2011.04.104.

[3] K. Mallick, D. Holland, Strengthening of container glasses by ion-exchange dip coating, J. Non-Cryst. Solids, 351 (2005) 2524-2536. DOI: 10.1016/j.jnoncrysol.2005.06.040.

[4] M. Cerruti, D. Greenspan, K. Powers, Effect of pH and ionic strength on the reactivity of Bioglass® 45S5, Biomaterials, 26 (2005) 1665-1674. DOI: 10.1016/j.biomaterials.2004.07.009.

[5] G. Greaves, S. Sen, Inorganic glasses, glass-forming liquids and amorphizing solids, Adv. Phys., 56 (2007) 1-166. DOI: 10.1080/00018730601147426.

[6] J.S. Sieger, Chemical characteristics of float glass surfaces, in: Glass Surfaces, Elsevier, 1975, pp. 213-220. DOI: 10.1016/0022-3093(75)90086-1.

[7] M. Grujicic, W.C. Bell, B. Pandurangan, B.A. Cheeseman, P. Patel, P.G. Dehmer, Effect of the tin- versus air-side plate-glass orientation on the impact response and penetration resistance of a laminated transparent armour structure, Proc. Inst. Mech. Eng. L, 226 (2012) 119-143. DOI: 10.1177/1464420711433991.

[8] J.A. Howell, J.R. Hellmann, C.L. Muhlstein, Nanomechanical properties of commercial float glass, J. Non-Cryst. Solids, 354 (2008) 1891-1899. DOI: 10.1016/j.jnoncrysol.2007.10.021.

[9] T. Rouxel, J.C. Sangleboeuf, C. Moysan, B. Truffin, Indentation topometry in glasses by atomic force microscopy, J. Non-Cryst. Solids, 344 (2004) 26-36. DOI: 10.1016/j.jnoncrysol.2004.07.020.

[10] M.H. Krohn, J.R. Hellmann, D.L. Shelleman, C.G. Pantano, G.E. Sakoske, Biaxial Flexure Strength and Dynamic Fatigue of Soda–Lime–Silica Float Glass, J. Am. Ceram. Soc., 85 (2002) 1777-1782. DOI: 10.1111/j.1151-2916.2002.tb00352.x.

[11] A. Barkatt, Glass - Science and Technology, Vol 5, Elasticity and Strength in Glasses - Uhlmann,Dr, Kreidl,Nj, J. Am. Chem. Soc., 105 (1983) 2510-2510.

[12] K. Takahashi, Fast fracture in tempered glass, in: Key Engineering Materials, Trans. Tech. Publ., 1999, pp. 9-18. DOI: 10.4028/www.scientific.net/KEM.166.9.

[13] L.A. Pilkington, Pilkington Group PLC, 1963. Manufacture of flat glass. U.S. Patent 3, 083, 551.

[14] P.M. Hogan, Brockway Glass Co Inc, 1980. Method of glass strengthening by ion exchange. U.S. Patent 4,218,230.

[15] V.M. Sglavo, Chemical Strengthening of Soda Lime Silicate Float Glass: Effect of Small Differences in the KNO_3 Bath, Int. J. Appl. Glass Sci. , 6 (2015) 72-82. DOI: 10.1111/ijag.12101.

[16] A.K. Varshneya, Chemical Strengthening of Glass: Lessons Learned and Yet To Be Learned, Int. J. Appl. Glass Sci., 1 (2010) 131-142.DOI: 10.1111/j.2041-1294.2010.00010.x.

[17] R.C. Welch, J.R. Smith, M. Potuzak, X. Guo, B.F. Bowden, T. Kiczenski, D.C. Allan, E.A. King, A.J. Ellison, J.C. Mauro, Dynamics of glass relaxation at room temperature, Phys. Rev. Lett., 110 (2013) 265901.. DOI: 10.1103/PhysRevLett.110.265901.

[18] S.M. Dockerty, G.C. Shay, Corning Inc, 1964. Downflow sheet drawing method and apparatus. U.S. Patent 3,149,949.

[19] X.Y. Li, L.B. Jiang, X.W. Zhang, Y. Yan, Influence of residual compressive stress on nanoindentation response of ion-exchanged aluminosilicate float glass on air and tin sides, J. Non-Cryst. Solids, 385 (2014) 1-8. DOI: 10.1016/j.jnoncrysol.2013.10.018.

[20] S. Karlsson, B. Jonson, C. Stalhandske, The technology of chemical glass strengthening - a review, Glass Technol.: Eur. J. Glass Sci. Technol., Part A, 51 (2010) 41-54

[21] P.V. Kolluru, D.J. Green, C.G. Pantano, C.L. Muhlstein, Effects of surface chemistry on the nanomechanical properties of commercial float glass, J. Am. Ceram. Soc., 93 (2010) 838-847. DOI: 10.1111/j.1551-2916.2009.03497.x

[22] A.S.H. Makhlouf, 1 - Current and advanced coating technologies for industrial applications, in: A.S.H. Makhlouf, I. Tiginyanu (Eds.) Nanocoatings and Ultra-Thin Films, Woodhead Publishing, 2011, pp. 3-23. DOI: https://doi.org/10.1533/9780857094902.1.3.

[23] E.V. Barrera, L. Ge, S. Biradar, P.H. Brogan, B.E. Rich, 2016. Nano-(Multifunctional) Solutions for Glass and Glass Products: Heterogeneous Nano-Self-Assembly and/or Coating. U.S. Patent Application 14/825,139.

[24] T. Dey, D. Naughton, Cheap non-toxic non-corrosive method of glass cleaning evaluated by contact angle, AFM, and SEM-EDX measurements, Environ. Sci. Pollut. R, 24 (2017) 13373-13383. DOI: 10.1007/s11356-017-8926-4.

[25] W. Eitel, Industrial glass: glazes and enamels, Elsevier, 2012.

[26] M.H. Krohn, J.R. Hellmann, B. Mahieu, C.G. Pantano, Effect of tin-oxide on the physical properties of soda-lime–silica glass, J. Non-Cryst. Solids, 351 (2005) 455-465. DOI: 10.1016/j.jnoncrysol.2005.01.050.

[27] K.F.E. Williams, C.E. Johnson, J. Greengrass, B.P. Tilley, D. Gelder, J.A. Johnson, Tin oxidation state, depth profiles of Sn^{2+} and Sn^{4+} and oxygen diffusivity in float glass by Mössbauer spectroscopy, J. Non-Cryst. Solids, 211 (1997) 164-172. DOI: 10.1016/S0022-3093(96)00636-9.

[28] G. Principi, A. Maddalena, A. Gupta, F. Geotti-Bianchini, S. Hreglich, M. Verita, Oxidation state of surface tin in an industrially produced float glass, Nucl. Instrum. Methods Phys. Res. B 76 (1993) 215-217. DOI: 10.1016/0168-583X(93)95185-8.

[29] L. Jie, X. Chao, XPS examination of tin oxide on float glass surface, J. Non-Cryst. Solids, 119 (1990) 37-40. DOI: 10.1016/0022-3093(90)90238-H.

[30] M. Dubey, I. Gouzman, S.L. Bernasek, J. Schwartz, Characterization of self-assembled organic films using differential charging in X-ray photoelectron spectroscopy, Langmuir, 22 (2006) 4649-4653. DOI: 10.1021/la053445f.

[31] R. Girard, A. Faivre, F. Despetis, Crack healing by thermal treatment in float glass: the effect of tin, J. Am. Ceram. Soc., 97 (2014) 3463-3468. DOI: 10.1111/jace.13140.

[32] B.O. Mysen, L.W. Finger, D. Virgo, F.A. Seifert, Curve-fitting of Raman spectra of silicate glasses, Am. Mineral., 67 (1982) 686-695.

[33] S.A. Brawer, W.B. White, Raman spectroscopic investigation of the structure of silicate glasses (II). Soda-alkaline earth-alumina ternary and quaternary glasses, J. Non-Cryst. Solids, 23 (1977) 261-278. DOI: 10.1016/0022-3093(77)90009-6.

[34] P. McMillan, Structural studies of silicate glasses and melts-applications and limitations of Raman spectroscopy, Am. Mineral., 69 (1984) 622-644.

[35] E. Kilinc, R.J. Hand, Mechanical properties of soda–lime–silica glasses with varying alkaline earth contents, J. Non-Cryst. Solids, 429 (2015) 190-197. DOI: 10.1016/j.jnoncrysol.2015.08.013.

[36] P. Colomban, A. Tournié, L. Bellot-Gurlet, Raman identification of glassy silicates used in ceramics, glass and jewellery: a tentative differentiation guide. J. Raman Spectrosc., 37 (2006) 841-852. DOI: 10.1002/jrs.1515

[37] M.T. Wang, J.S. Cheng, B. Li, F. He, Raman spectra of soda-lime-silicate glass doped with rare earth. Physica B, 406 (2011) 3865-3869. DOI: 10.1016/j.physb.2011.07.014.

[38] Y. Tsunawaki, N. Iwamoto, T. Hattori, A. Mitsuishi, Analysis of CaO-SiO_2 and CaO-SiO_2-CaF_2 glasses by Raman spectroscopy. J. Non-Cryst Solids, 44 (1981) 369-378. DOI: 10.1016/0022-3093(81)90039-9.

[39] C. Calahoo, J.W. Zwanziger, I.S. Butler, Mechanical–structural investigation of ion-exchanged lithium silicate glass using micro-Raman spectroscopy, J. Phys. Chem. C, 120 (2016) 7213-7232. DOI: 10.1021/acs.jpcc.6b01720.

[40] D.W. Matson, S.K. Sharma, J.A. Philpotts, The structure of high-silica alkali-silicate glasses. A Raman spectroscopic investigation, J. Non-Cryst. Solids, 58 (1983) 323-352. DOI: 10.1016/0022-3093(83)90032-7.

[41] P. Colomban, Polymerization degree and Raman identification of ancient glasses used for jewelry, ceramic enamels and mosaics, J. Non-Cryst. Solids, 323 (2003) 180-187 DOI: 10.1016/S0022-3093(03)00303-X.

[42] A. Koike, S. Akiba, T. Sakagami, K. Hayashi, S. Ito, Difference of cracking behavior due to Vickers indentation between physically and chemically tempered glasses, J. Non-Cryst. Solids, 358 (2012) 3438-3444. DOI: 10.1016/j.jnoncrysol.2012.02.020